IEEE Open Journal of the
Industrial Electronics Society

Received 19 November 2024; accepted 20 December 2024. Date of publication 24 December 2024;
date of current version 9 January 2025. The review of this article was arranged by Associate Editor Saeed Golestan.

Digital Object Identifier 10.1109/OJIES.2024.3521972

Complex-Order Fractional Proportional–Resonant Controller for High-Frequency Applications

DANIEL HEREDERO-PERIS [1], MACIÀ CAPÓ-LLITERAS [1], DANIEL MONTESINOS-MIRACLE [1] (Senior Member, IEEE), AND JOAQUIM MELENDEZ-FRIGOLA [2]

[1]Centre d'Innovació Tecnològica en Convertidors Estàtics i Accionaments, Departament d'Enginyeria Elèctrica, Escola Tècnica Superior d'Enginyeria Industrial de Barcelona, Universitat Politècnica de Catalunya, 08028 Barcelona, Spain
[2]Grup de Recerca en Enginyeria de Control i Sistemes Intel.ligents, Institut d'Informàtica i Aplicacions, Department Enginyeria Elèctrica, Electrònica i Automàtica, Universitat de Girona, 17003 Girona, Spain

CORRESPONDING AUTHOR: DANIEL HEREDERO-PERIS (e-mail: daniel.heredero@upc.edu).

ABSTRACT This article presents the design and implementation of a complex-order fractional proportional–resonant (COFPR) controller. The proposed COFPR controller is an evolution of the fractional proportional–resonant (FPR) controller suitable for high-frequency tracking. The best performance of the COFPR controller is obtained by reducing the excitation region promoted by FPR controllers and proportional–resonant (PR) controllers. The COFPR controller is analyzed in the frequency domain. For comparison purposes, proportional–resonant with harmonic compensator, FPR, and COFPR controllers are designed for the current regulation of a voltage-source converter. They are compared considering the same controller gain tuning criteria and the same phase margin. A set of simulations and experimental results on a 3.6-kVA gallium nitride inverter is discussed. The proposed COFPR controller performs superiorly at high frequencies when the same gains for the controllers are used. The COFPR controller can reduce excitation regions in PR controllers tuned with a similar phase margin without losing close tracking capability. This advantage promotes the COFPR controller as a proper alternative regarding program memory and execution time required, as it can be properly implemented within a specific frequency range by an approximation of third or fourth order.

INDEX TERMS Current control, fractional exponents, grid-following inverters, resonant controllers.

NOMENCLATURE

∼	Approximation.
AC	Alternative current.
COFPR	Complex-order fractional proportional–resonant.
COFR	Complex-order fractional resonant.
COPID	Complex-order proportional–integral–derivative.
CO	Complex-order.
DC	Direct current.
DSP	Digital signal processor.
FOC	Fractional-order control.
FPR	Fractional proportional–resonant.
FR	Fractional resonant.
GaN	Gallium nitride.
GM	Gain margin.
HC	Harmonic compensator.
IMC-CFOPID	Internal model control complex fractional-order proportional integral derivative.
IMC	Internal model control.
Mod-CFOPID	Modified internal model control complex fractional-order proportional integral derivative.
PD	Proportional derivative.
PID	Proportional integral derivative.
PIHC	Proportional integral with harmonic compensator.
PI	Proportional integral.

PLL	Phase-locked loop.
PM	Phase margin.
PRHC	Proportional–resonant with harmonic compensator.
PR	Proportional–resonant.
RO	Real order.
VSC	Voltage-source converter.
ZOH	Zero-order hold.

I. INTRODUCTION

Alternative magnitude tracking, such as voltage and current in VSCs, poses significant challenges that are crucial for industrial applications, such as active filters, integration, and battery–grid integration, among others.

Many control strategies have been developed to address these challenges, including hysteresis control, IMC, and rotating reference frame control [1], [2], [3]. However, PI and PR controllers are more commonly used controllers for regulation. Furthermore, PI and PR controllers are known for their narrow bandwidth control capabilities, making them selective to tuned frequency tones [4], [5]. One extended strategy to overcome the PI limitations is to use a synchronous reference frame to move ac magnitudes into dc [6]. This is done using PLL algorithms. However, conventional PLLs are limited to a single frequency value and determine the outcome dynamics [7], [8]. Various approaches, such as the use of PIHC or PRHC, have been proposed to mitigate the mentioned bandwidth narrowness [9], [10], [11]. These alternatives increase complexity, computational burdens, and tuning difficulties, impacting the stability and robustness analysis.

Fractional calculus, introduced in control in the late 1990s, offers additional degrees of freedom for control objectives. Fractional-order calculation, dating back to Leibniz and Hôpital in 1695, utilizes noninteger orders, including complex values [12]. FOC has been applied to improve modeling, enhance control, and provide additional degrees of freedom [13], [14], [15]. Recent efforts focus on robust tuning criteria and industrialization of FOC controllers [15], [16], [17], [18].

In ac regulation applied to VSCs, FOC has shown promise, as seen in examples that improve time response and disturbance rejection in PI controllers [19], [20], [21], [22]. The FPR controller was introduced in 2016 [23] and later renamed as fractional ideal PR controller in 2021 [24]. Studies have shown how FPR increases control bandwidth with a lower computational burden compared to PRHC controllers [25]. The existing studies primarily focus on current regulation [21], [24], [25]. However, FPR controllers present an excitation region where certain frequency components are coupled to the desired output current. This consequence impacts the quality of the delivered current.

This article aims to extend the use of FOC controllers, focusing on the current ac regulation challenge. In this case, an extended formulation for the FR controller is proposed based on the form $s^{\alpha}/(s^2+\omega_0^2)$. In the FR conventional form, α is a real value, and ω_0 corresponds to the desired resonant frequency. The proposed extension uses a complex exponent for the s^{α}-Laplace variable, becoming s^{γ} with γ constituted by real and complex terms. This way, the COFPR controller is defined when proportional and integral gains are added to the FPR controller, assuming s^{γ}. Results demonstrate that the COFPR controller can better track high frequencies without losing tracking capability at the low-frequency range compared with FPR controllers. Moreover, the COFPR controller overcomes the excitation region issue of RO-FPR, PR, or PRHC controllers. This enhancement is achieved using a COFPR controller with a lower order blue or similar order compared to an equivalent PRHC when the same controller gains or the same PMs are imposed. The low-order implementation enables the use of this controller in applications where cyclic execution time is critical.

The rest of this article is organized as follows. Section II introduces the contribution of this article. This section defines the state of the art of noninteger controllers, poses the basics of CO s-Laplace operators, and proposes the COFPR controller and the plant to which the COFPR controller is applied. Section III presents a control analysis based on the frequency domain and exposes a procedure to obtain the approximated form of the controller. Section IV stages the simulated and experimental tests, followed by a qualitative discussion of the results in Section V. Finally, Section VI concludes this article.

II. CONTRIBUTION

A. STATE OF THE ART OF NONINTEGER CONTROLLERS

A COFPR controller is an extension of the FR controller based on the $s^{\alpha}/(s^2+\omega_0^2)$ transfer function. The extension is achieved by expanding the orders of the derivative term to include complex numbers and by including gains on the controller.

Many control applications have exploited fractional-order controllers to achieve new controller formulas. This fractional alternative opens new degrees of freedom usable for tuning purposes. A summary table of the FOC formulas used by different authors in control applications can be seen in Table 1 [12], [25], [26], [27]. In Table 1, the orders n, λ, μ, and α of controller actions are real numbers in the range of 0 and 2, the term k_x represents the controller gains, and ω_x represents angular pulsations used for tuning purposes. Only IMC-CFOPID, Mod-CFOPID, and COPID controllers explore the use of the imaginary part on the operator s^x. The authors proposing to use CO on the s-Laplace operator have concluded that these controllers outperform the real equivalent controllers but increase the complexity of the design process. This difficulty resides in extra degrees of freedom to tune and use approximations to obtain a programmatic form.

To the best of the authors' knowledge, as seen in Table 1, there are no existing studies on applying CO forms to resonant controllers, as proposed in this article. Consequently, introducing the complex term provides new opportunities to utilize an additional degree of freedom for managing the system's frequency response.

TABLE 1. State of the Art of Noninteger Controllers

Author	Controller	Transfer Function	Remark
A. Oustaloup	CRONE derivative	$k_d s^{\alpha}$	RO [1]
A. Oustaloup	CRONE integrator	$k_i \frac{1}{s^{\alpha}}$	RO
I. Poudlubny	PI$^{\lambda}$	k_p+k_i/s^{λ}	RO
	PID$^{\mu}$	$k_p+k_i/s+k_d s^{\mu}$	RO
	PI$^{\lambda}$D$^{\mu}$	$k_p+k_i/s^{\lambda}+k_d s^{\mu}$	RO
M. Tenoutit	(PI)^n	$s^{-n}(k_p+k_i/s^{\lambda})$	RO
	(PD)^n	$s^{-n}(k_p+k_i s^{\mu})$	RO
	(PID)^n	$s^{-n}(k_p+k_i/s^{\lambda}+k_d s^{\mu})$	RO
Tavakoli	IMC-FOPID	$k_p+k_i/s^{\alpha}+\frac{k_d s^{\alpha}}{\gamma s^{\alpha}+1}$	RO
Luo	(PI)$^{\lambda}$	$(k_p+k_i/s)^{\lambda}$	RO
	(PD)$^{\mu}$	$(k_p+k_d s)^{\lambda}$	RO
El-Khazali	Mod-FOPID	$k_c \frac{(1+T_i s^{\mu})^2}{s^{\mu}}$	RO
F. Merrikh-Bayat	Non-Linear FOPID	$k_d\|D^{\mu}e(t)\|^{\beta} sign(D^{\mu}e(t))+$	RO
		$+k_i\|D^{\lambda}e(t)\|^{\gamma} sign(D^{\lambda}e(t))$	RO
D.Heredero	FPR	$k_p+k_i \frac{s^{\alpha}}{s^2+\omega_0^2}$	RO
D. Xue	Fractional Lead-Lag	$\left(\frac{1+s/\omega_b}{1+s/\omega_h}\right)^r$	RO
O.W. Abdulwahhab	COPID	$k_p+k_i/s^{\alpha+\beta j}+k_d s^{\alpha+\beta j}$	CO [2]
Bingi	IMC-CFOPID	$k_p+k_i/s^{\alpha+\beta j}+\frac{k_d s^{\alpha+\beta j}}{\gamma s^{\alpha+\beta j}+1}$	CO
	Mod-CFOPID	$k_c \frac{(1+T_i s^{\alpha+\beta j})^2}{s^{\alpha+\beta j}}$	CO
D. Heredero	COFPR (**Proposal**)	$k_p+k_i \frac{s^{\alpha+\beta j}}{s^2+\omega_0^2}$	CO

[1]Real Order
[2]Complex Order

B. BASICS OF THE COMPLEX FRACTIONAL-ORDER OPERATOR s^{γ}

The fractional-order γ differentiator in the Laplace domain is typically defined by

$$G_d(s) = s^{\gamma} \tag{1}$$

with γ being described by $\alpha + j\beta$. Note that (1) comes from

$$\mathcal{L}\{{}_aD_t^{\gamma} f(t); s\} = s^{\gamma} F(s) \tag{2}$$

where

$${}_aD_t^{\gamma} f(t) = \frac{1}{\Gamma(n-\alpha)} \frac{d^n}{dx^n} \int_a^x (x - t^{n-\alpha-1}) f(t) dt \tag{3}$$

as indicated in [28]. When dealing with COs, the derivative may show oscillatory characteristics because of the imaginary component (β), while the fractional part introduces memory effects (α). Integrating fractional order and CO makes operators responsive to functions' local and overall properties, allowing them to capture finer details of a function's behavior over a given range. These properties can be applied to the control theory, obtaining new and advanced dynamic system responses or novel modeling alternatives.

The corresponding isochronous form from (1) is

$$G_d(j\omega) = j^{\alpha}\omega^{\alpha} e^{-\beta\frac{\pi}{2}} (\cos(\beta \ln \omega) + j \sin(\beta \ln \omega)). \tag{4}$$

From (4), it is possible to analyze the effect on the frequency behavior when α and β are swept in [0, 1] and [−1, 1], respectively. For easy understanding, in Figs. 1 and 2, only one of the complex γ components, α or β, is swept. On the one hand, when β is null, the module of (4) yields

$$|G_d(j\omega)| = \omega^{\alpha} \text{ [abs]} \tag{5}$$

while the phase is

$$\arg(G_d) = \alpha \frac{\pi}{2} \text{ [rad]}. \tag{6}$$

On the other hand, when α is null, the magnitude is defined by

$$|G_d(j\omega)| = e^{-\beta\frac{\pi}{2}} \text{ [abs]} \tag{7}$$

and the phase by

$$\arg(G_d(j\omega)) = \beta \ln(\omega) \text{ [rad]}. \tag{8}$$

It can be deduced that any fractional alternative provides an extra degree of freedom to modify the frequency response of the system from (5) to (8). The α and β components allow the modification of the phase in a controlled way to use this variability to lead or lag the delay introduced by the controller. In terms of gain, the α term introduces an increasing gain over the frequency, while the β term manages the controller gain constantly in the full frequency range.

C. PROPOSED COFPR CONTROLLER

A causal RO-FR controller, i.e., $\alpha \leq 2$, with the transfer function

$$G_{FR}(s) = \frac{s^{\alpha}}{s^2 + \omega_0^2} \tag{9}$$

is used as the basis for its extended version, the COFR controller. First, Fig. 3 recalls the affectation of α with null β in the frequency domain when ω_0 is set to 100π rad/s [25]. It can be deduced from Fig. 3 that positive α values help to hugely increase the gain in the vicinity of ω_0. In terms of phase, positive α values lead the phase response at all the

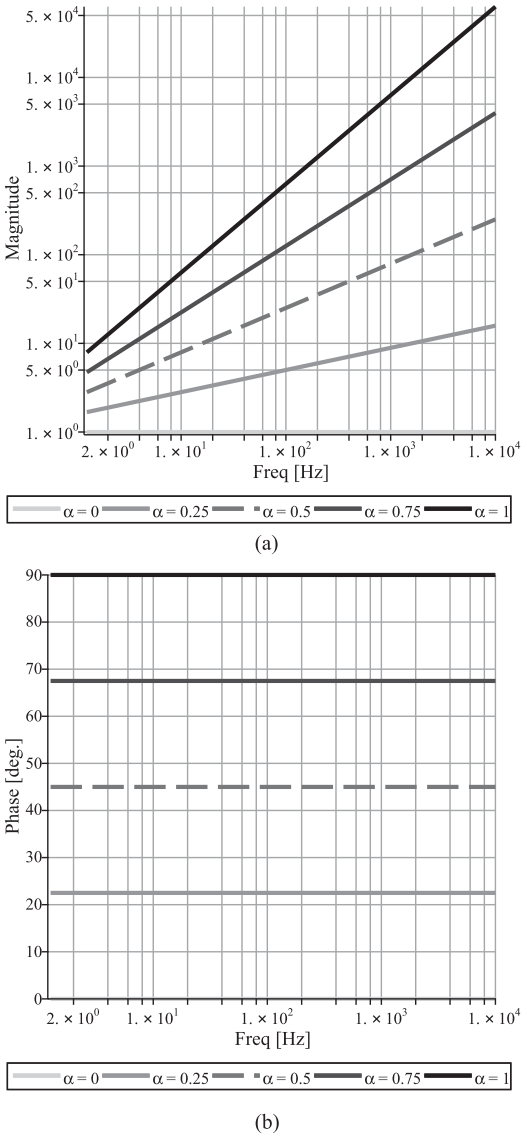

FIG. 1. Bode diagrams for s^{α}, $\alpha \in [0, 1]$. (a) Gain. (b) Phase.

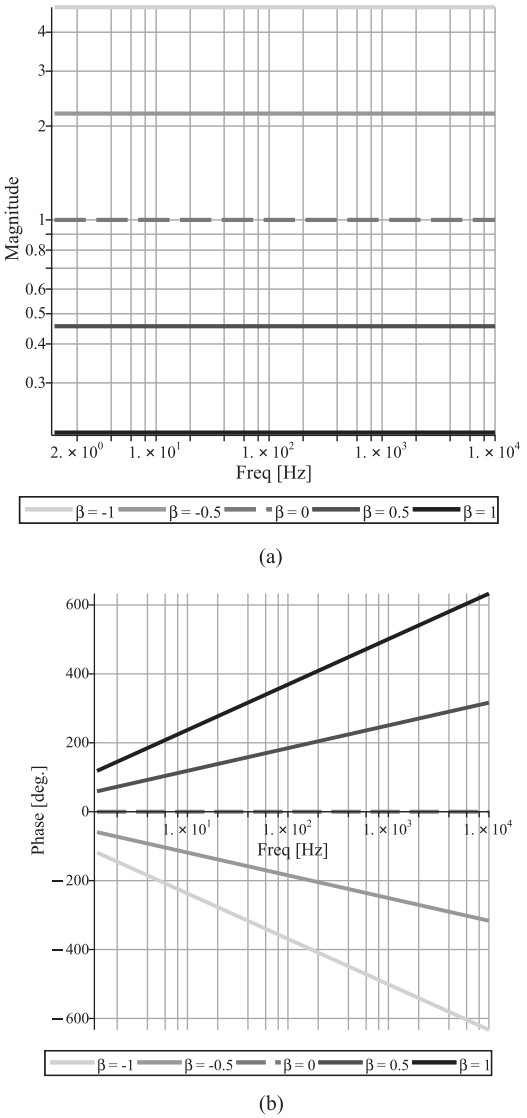

FIG. 2. Bode diagrams for $s^{j\beta}$, $\beta \in [-1, 1]$. (a) Gain. (b) Phase.

frequency ranges, as introduced by (6). Strictly, the phase of the FR controller is modified concerning a conventional PR controller by

$$\phi_{\text{FR}} = \phi_{\text{PR}} + \alpha \frac{\pi}{2} \, [\text{rad}] \, . \tag{10}$$

Once the FR controller is outlined, the COFR controller can be defined and analyzed. Thus, the FR controller is expanded to a COFR controller as

$$G_{\text{COFR}}(s) = \frac{s^{\alpha + j\beta}}{s^2 + \omega_0^2} . \tag{11}$$

As presented in Section II-B, the inclusion of the imaginary part to (9) adds high nonlinearity. Due to this high nonlinearity, the Bode diagram of the COFR controller is presented in two ranges: β from -1 to 1 (see Fig. 4) and β from -0.1 to 0.1 (see Fig. 5). The α value is held constant and set to 1.5. Similar conclusions can be deduced for any $\alpha \in (1, 2)$. Thus, from Fig. 4, it can be concluded that positive β values increase the full range gain at both sides of ω_0, while negative values produce the opposite effect. This effect is similar to the one obtained using the α component. However, using the imaginary β component affects the phase response more intensively. It can be seen in Fig. 4 that it is not possible to define a unique lag/lead behavior corresponding to the β value itself, not even due to the sign of β. However, if β is small enough, i.e., $\beta < |0.1|$, some deductions can be drawn (see Fig. 5). When β is small, the COFR controller offers a sign bias resonance phase at ω_0. This bias matches in sign with the polarity of β. Also, the phase always increases or decreases in absolute terms according to the sign of β: the positive sign indicates that the phase increases, and the negative sign indicates that it decreases.

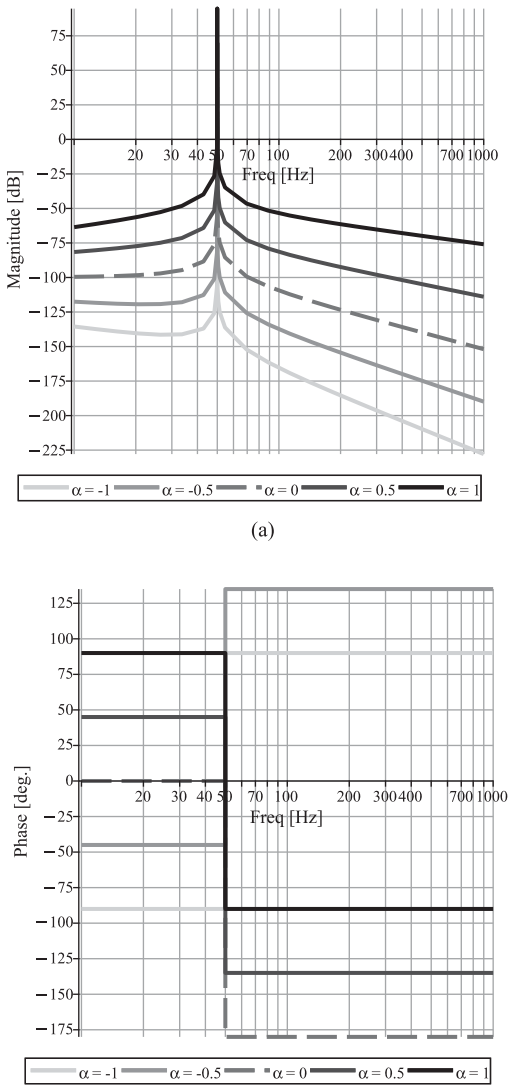

FIG. 3. Bode diagrams of (9) for $\alpha \in [-1, 1]$. (a) Gain. (b) Phase.

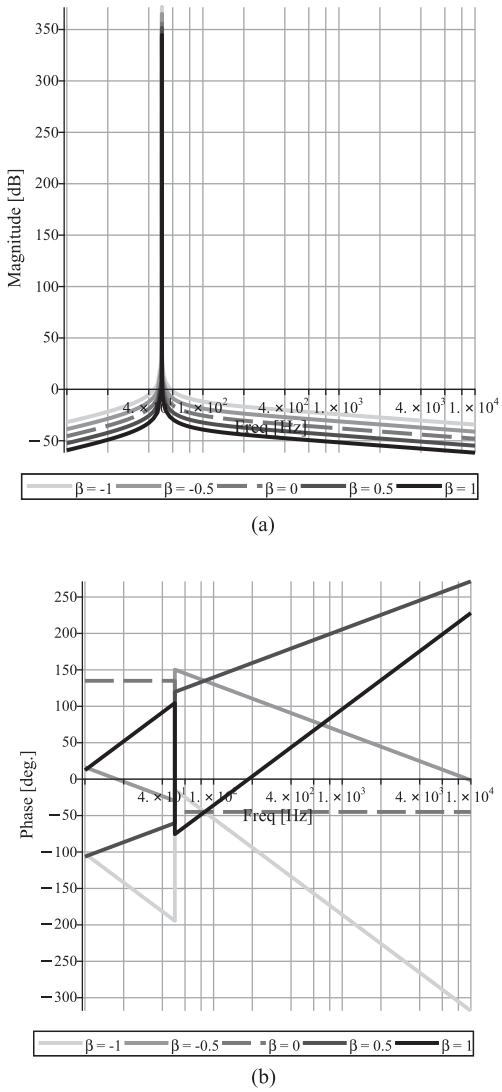

FIG. 4. Bode diagrams for the COFR controller of (11) for $\beta \in [-1, 1]$. (a) Gain. (b) Phase.

Finally, once the effect of a complex noninteger FR controller is analyzed, the COFPR controller emerges as

$$G_{\text{COFPR}}(s) = k_p + k_i \frac{s^{\alpha+j\beta}}{(s^2 + \omega_0^2)} \tag{12}$$

where k_p and k_i are the corresponding controller gains.

D. MATHEMATICAL MODEL OF THE PLANT

The proposed COFPR controller will be designed to control the output current of an inverter, $i_L(t)$. This current flows through an inductive coupling filter with a transfer function

$$G_p(s) = \frac{I_L}{V_s}(s) = \frac{1}{Ls + R_L} \tag{13}$$

where L is the inductance (in henries), R_L is the equivalent series resistance of L (in ohms), $I_L(s)$ is the current through the inductance (in amperes), and $V_s(s)$ is the voltage drop of the inductance (in volts).

For computations, and without loss of generality, it will be considered a real system with specific parameters as a case study. This system is the output inductive filter of a GaN inverter switched at 120 kHz. Upon identifying the system, its parameters are defined by $L = 80\ \mu$H and $R_L = 10\ \text{m}\Omega$. As the control of the GaN inverter will be intrinsically discrete, (13) is converted to discrete using ZOH transformation, yielding

$$G_p(z) = \frac{e^{R_L T_s/L} - 1}{R_L \left(e^{R_L T_s/L} z - 1\right)} = \frac{0.10384}{z - 0.9938} \tag{14}$$

for further validation.

Note that according to [29] and [30], the phase lag caused by the inductive filter almost reaches a constant value of $\pi/2$ rad a decade above a frequency named as f_{90}. This

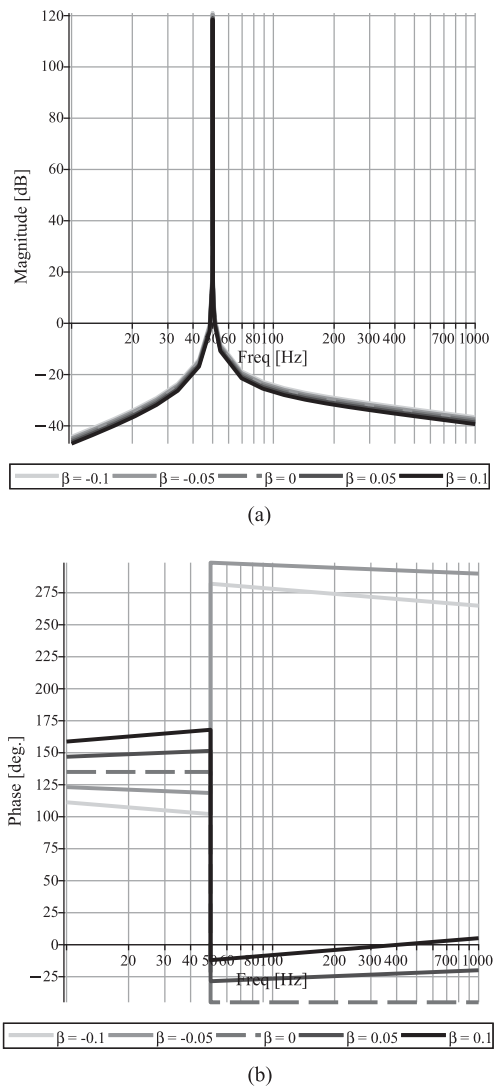

FIG. 5. Bode diagrams for the COFR controller of (11) for $\beta \in [-0.1, 0.1]$. (a) Gain. (b) Phase.

frequency can be computed as

$$f_{90}[\text{Hz}] = \frac{5R_L}{L}. \tag{15}$$

f_{90} results in more than 4 kHz for the selected parameters. Also, in [29] and [30], it is exposed that two samples are required to compensate the phase for solving instability problems that appear for

$$\frac{f_1 h}{f_s} > 0.1 \tag{16}$$

where h is the harmonic component, f_1 is the fundamental frequency, and f_s is the sampling frequency. In this case, h is 240, i.e., the phase for solving instability will start at about 12 kHz. Since the control bandwidth will be focused on frequencies below 12 kHz, the phase compensation of the plant is not considered in this work.

TABLE 2. List of Controllers Used for Comparison Reasons

Option	Transfer function
COFPR	$k_1+k_2\frac{s^{\alpha+j\beta}}{s^2+\omega_0^2}$
FPR	$k_1+k_2\frac{s^{\alpha}}{s^2+\omega_0^2}$
PRHC	$k_1+\sum_{n=0}^{n=3}\frac{k_2}{2n+1}\frac{s}{s^2+((2n+1)\omega_0)^2}$

III. ANALYSIS AND DESIGN

A. FREQUENCY-DOMAIN ANALYSIS BASED ON THE SAME CONTROLLER GAINS

This section aims to analyze the closed-loop tracking capability of the proposed COFPR in contrast with two other controllers, i.e., an FPR controller and a PRHC controller, all listed in Table 2.

In this section, all controllers consider the same gains. This approach enables the evaluation of the controllers' intrinsic properties, establishing a consistent and common baseline for control performance across different controllers. All the controllers will use k_1 set at 2, k_2 set at 200, and ω_0 set at 100π rad/s. These gains have been obtained following the procedure described in [31] for PR controllers. In [31], it is described as an option to tune the PR controllers using the desired dynamic at 50 Hz. Then, the settling time for 50 Hz is set to 0.3 ms and the damping coefficient to 0.45 (low damping factors are adequate for grid synchronization [30]). The harmonic components are tuned by scaling the fundamental gain according to the harmonic order (n). Since the fundamental frequency typically carries the most significant portion of the signal's power, dividing the harmonic gains by the factor n ensures that the components are properly balanced and not overcompensated relative to the fundamental frequency.

Furthermore, for the FPR and COFPR controllers, the α value is common and set at 1.5. A procedure to select a proper α can be found in [25]. In this case, the α value of 1.5 results in a tradeoff between evolving a PR controller into an FPR one without compromising in excess the stability margins.

As described in Table 2, the PRHC controller uses n equal to 3, which means 50, 150, 250, and 350 Hz. This results in a controller of order 8, whereas the FPR and COFPR controllers are ideally of order 2. As mentioned, the PRHC controller only achieves controlled tones up to 350 Hz. To maintain a consistent comparison criterion based on controller order, no more HCs are considered. Also, it could be possible to replace one low-order HC for a high-order HC, for example, replacing n equal to 3 in Table 2 to 20. In this last case, phase compensation is required. However, this will affect the phase tracking capability between n equal to 2 and 19.

1) TRACK CAPABILITY AND FREQUENCY RESPONSE

Figs. 6 and 7 show the continuous-time closed-loop Bode diagrams for the plant defined in (13) and the proposed controllers. In Fig. 6, the β values considered are close to the null value. Thus, the nonlinearity promoted by the complex term is reduced. A positive β value near zero helps to reduce

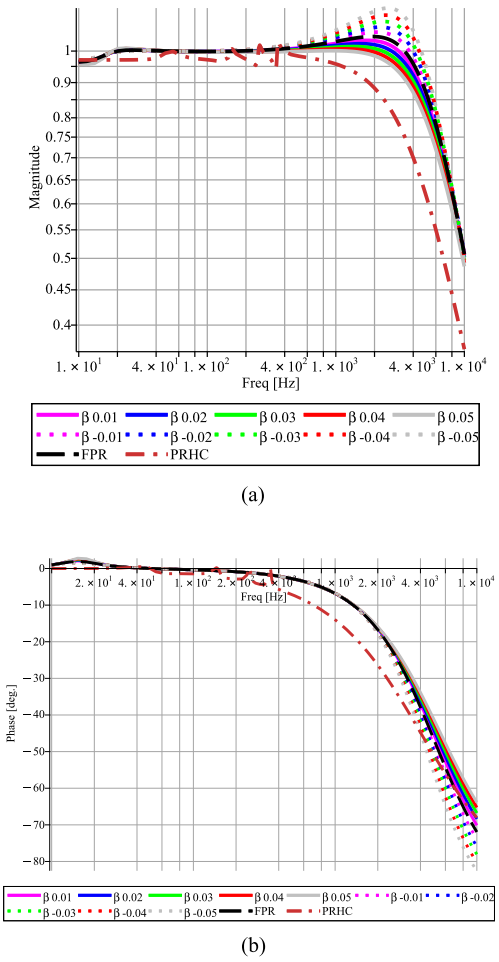

FIG. 6. Closed-loop Bode diagrams for the COFPR controller with $\alpha = 1.5$, $\beta \in [-0.05, 0.05]$, $k_1 = 2$, and $k_2 = 200$. (a) Gain. (b) Phase.

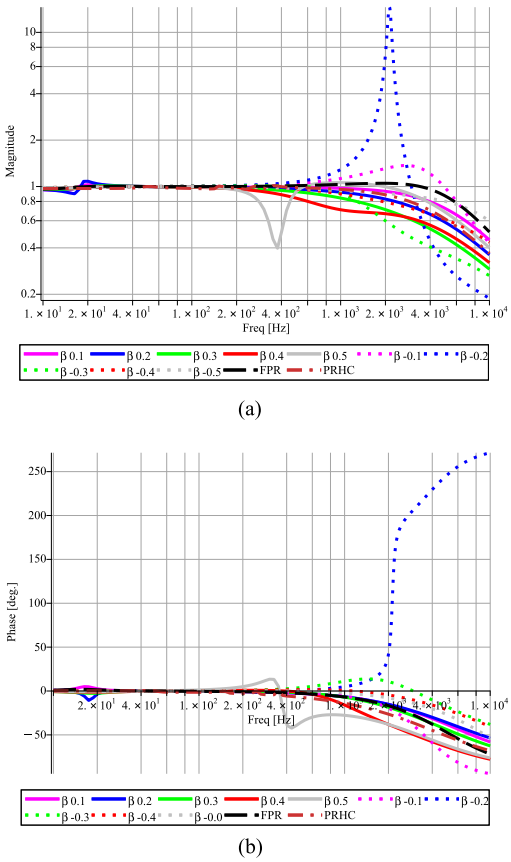

FIG. 7. Closed-loop Bode diagrams for the COFPR controller with $\alpha = 1.5$, $\beta \in [-0.5, 0.5]$, $k_1 = 2$, and $k_2 = 200$. (a) Gain. (b) Phase.

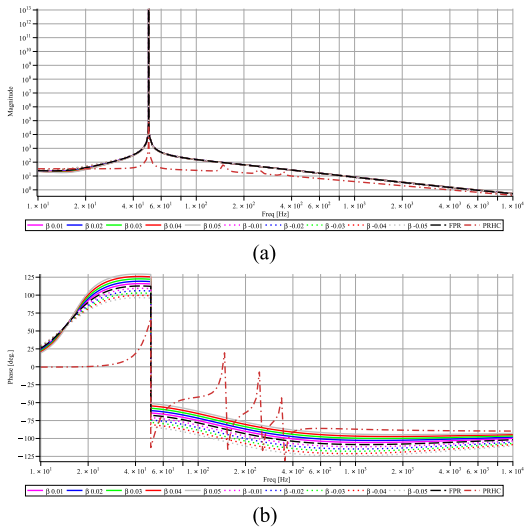

FIG. 8. Open-loop Bode diagrams for the COFPR, FPR, and PRHC controller with $\alpha = 1.5$, $\beta \in [-0.05, 0.05]$, $k_1 = 2$, and $k_2 = 200$. (a) Gain. (b) Phase.

the excitation region promoted by FPR controllers with a minimum affectation in the phase response. In Fig. 7, it can be observed how the nonlinearity introduced by higher β values produces a change in the closed-loop response that cannot be analyzed practically. For β higher than $|0.1|$, it is proposed to draw the closed-loop Bode diagram and analyze the feasibility of the controller in terms of stability and robustness case by case. All COFPR or FPR controllers are superior in gain and phase tracking over traditional PRHC controllers if the same controller gains are considered. Furthermore, from Figs. 6 and 7, it can be deduced that the PRHC controller defines an interexcitation and big delay outside the tuned harmonic frequency tones to track.

2) STABILITY

This section analyzes the effect of including the complex term β in terms of stability. For this purpose, the corresponding open-loop Bode diagrams from the frequency analysis proposed in Section III-A1 are depicted in Fig. 8. Strictly, it is only considered the case where the β term is near the null value, as shown in Fig. 6. This scenario responds to the case where the behavior is more linear. The stability margins, GM and PM, are shown in Table 3, obtained from Fig. 8 are collected. In all cases, the GM is infinite. There is a trend for positive β values to increase the PM. In contrast, negative β values reduce the PM. For the case under study, from Fig. 8,

TABLE 3. GM and PM for Different β Values When Used in COFPR and FPR Controllers

β	GM	PM	Frequency$_{PM}$
0.01	∞	78.2 deg	36009 Hz
0.02	∞	80.2 deg	36322 Hz
0.03	∞	82.3 deg	36553 Hz
0.04	∞	84.3 deg	36702 Hz
0.05	∞	86.3 deg	36771 Hz
0 (FPR)	∞	75.9 deg	35614 Hz
-0.01	∞	73.8 deg	35134 Hz
-0.02	∞	71.6 deg	34570 Hz
-0.03	∞	69.3 deg	33922 Hz
-0.04	∞	67.1 deg	32189 Hz
-0.05	∞	64.7 deg	32373 Hz

which also includes the PRHC controller, the GM and PM are close to the case where β is 0.05.

B. FREQUENCY-DOMAIN ANALYSIS BASED ON THE SAME PM

This section aims to analyze the closed-loop tracking capability of the proposed COFPR in contrast with a PR controller tuned by PM criteria. By implementing this alternative tuning approach to the method presented in Section III-A, we facilitate a comparison with a minimum-order PR controller designed to maintain a specified PM. This comparison offers valuable insights into the robustness characteristics of the COFPR controller in relation to the PR controller.

Considering the PR controller defined by (12) when α is 1 and β is null, and the plant system defined by (13), it is possible to compute [32]

$$G_c(j\omega)G(j\omega) = e^{-j\pi-\phi_m} = \cos(\phi_{\mathrm{m}}) - j\sin(\phi_{\mathrm{m}}) \quad (17)$$

where $G_c(j\omega)$ represents the controller transfer function in the frequency domain, $G(j\omega)$ is the controller, and ϕ_m is the desired PM. Thus, (17) defines an equation that can be applied to obtain the controller's gains for a desired PM at a specific frequency ω set at ω_{PM}. Thus, the PR controller proportional gain tuned by the PM can be computed as

$$k_{p_{\mathrm{PM}}} = -\cos(\phi_{\mathrm{m}})R_L + \sin(\phi_{\mathrm{m}})L\omega_{\mathrm{PM}} \quad (18)$$

while the integral gain is

$$k_{i_{\mathrm{PM}}} = \frac{(\omega_{\mathrm{PM}}^2 - \omega_0^2)(\sin(\phi_{\mathrm{m}})R_L + \cos(\phi_{\mathrm{m}}))L\omega_{\mathrm{PM}}}{\omega_{\mathrm{PM}}}. \quad (19)$$

The COFPR controllers use the gains tuned at Section II-I-A, i.e., k_p equal to 2 and k_i equal to 200. From Fig. 8, it is possible to see that the PM of the open loop results in about 85° at 1 kHz when α is set to 1.5 and β is selected to be 0.05 for the mentioned controller gains. From this consideration, two specifications are defined.

1) Taking 1 kHz as ω_{PM} and assuming 85° as ϕ_m, it is possible to compare the COFPR and a simple PR of order 2 in terms of stability by fixing a controllability desired window up to 1 kHz. Considering (18) and (19), the PR is tuned obtaining a $k_{p_{\mathrm{PM}}}$ equal to 0.49 and a $k_{i_{\mathrm{PM}}}$ equal to 649.2.

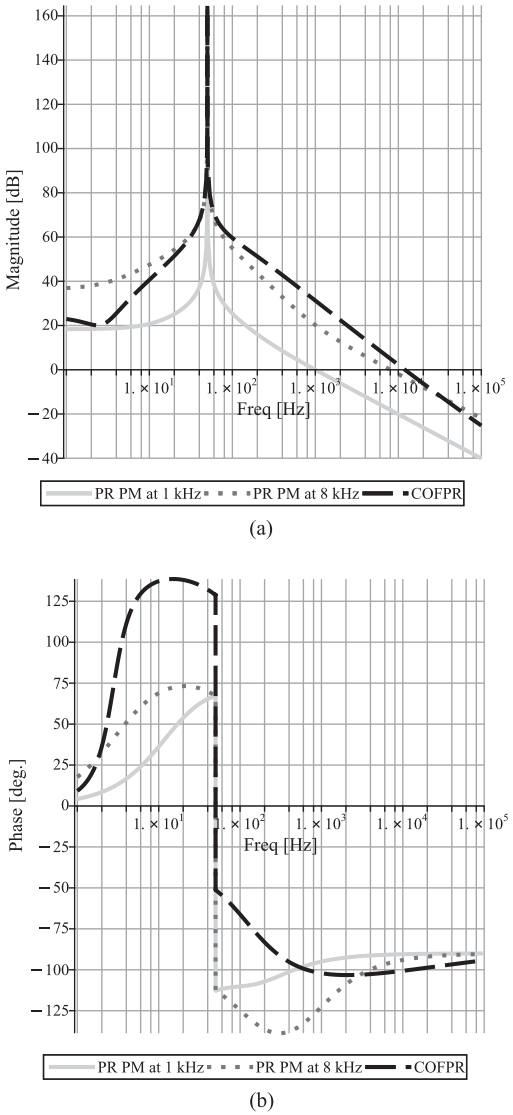

FIG. 9. Bode diagrams of the open-loop system for PR controllers tuned under PM criteria and COFPR controller tuned according to Section III-A. (a) Gain. (b) Phase.

2) Increasing ω_{PM} to 8 kHz is also proposed, maintaining the PM at 85°. This frequency of 8 kHz has been considered because, as seen in Fig. 8, the phase starts to be flat from this frequency tone. In this case, $k_{p_{\mathrm{PM}}}$ is equal to 4.0 and a $k_{i_{\mathrm{PM}}}$ is equal to 20 620.

Figs. 9 and 10 represent the open- and closed-loop bode diagrams comparing the COFPR controller tuned in Section III-A and the two PR controllers tuned by PM criteria at 1 and 8 kHz, respectively. In Fig. 9, it can be seen that the COFPR and PR controllers tuned when ω_{PM} is equal to 1 kHz match at that frequency in terms of GM. In contrast, the PR controller tuned at ω_{PM} equal to 8 kHz presents the desired PM at 8 kHz but offers lower stability margins from 50 Hz to 3 kHz than the COFPR controller and the PR controller tuned at 1 kHz by

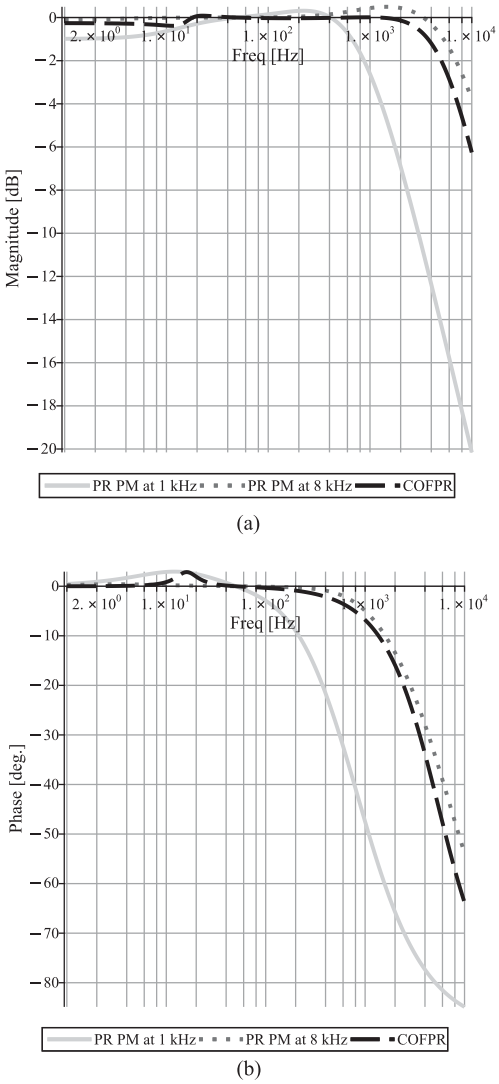

FIG. 10. Bode diagrams of the closed-loop system for PR tuned under PM criteria. (a) Gain. (b) Phase.

PM. Moreover, as shown in Fig. 10, when the frequency analysis is moved to the closed-loop point of view, it is possible to observe that the PR tuned by PM at 8 kHz presents better overall behavior. However, the COFPR nullifies the excitation regions. Note that this excitation region is about 0.5 dB at 1500 Hz on the PR controller tuned at 8 kHz by PM and for the study case.

C. APPROXIMATION FORM FOR THE COFPR CONTROLLER

The primary challenge with noninteger controllers is their lack of direct implementability. Consequently, from a mathematical perspective, they can only be analyzed in the frequency domain, as discussed in the preceding sections. Therefore, any noninteger controller must be approximated [12], [33]. Thus, this approximation procedure is required for any application, in which a fractional controller, real or complex, needs to be implemented; such is the case of using fractional controllers for power electronics [15], [34]. The step-by-step process for designing the controller is proposed as follows.

1) Plot the closed-loop bode diagrams and get one β value that satisfies the desired frequency response regarding gain and phase.
2) Choose a frequency range, $[\omega_l, \omega_h]$, to calculate an approximation for the proposed noninteger controller within the selected range and define an order N for the approximation.
3) From steps 1 and 2, obtain the frequency response data, H, i.e., for each pair [frequency (f), magnitude (M)] and [frequency (f), phase (ϕ)] to compute

$$H = M \cdot e^{\mathbf{j}\phi}. \tag{20}$$

4) Create frequency response data H models to convert dynamic system models to a frequency response data model format.
5) Use an optimization process or tool to obtain the desired approximation from H and order N. For the following sections, the μ-synthesis method is used for the approach of H. This technique is commonly used for robust control system design for an uncertain plant.
6) Compare and validate if the approximation is accurate enough for a desired frequency range. This frequency range can be different from $[\omega_l, \omega_h]$, but it should be contained in the last one.
7) Check the system stability with the obtained approximation in the last step.

Steps 4–6 can be substituted by any other preferred approximation, as suggested in [33]. For example, Oustaloup's or Carlson's approximations are possible approximations based on rational recursive formulation and Newton's-based iterative formulas to approximate the controller's transfer function. However, these alternatives are only valid for the real part of the complex FR controller.

Treating the stability issue from an analytical perspective is tedious due to the high nonlinearity of the COFPR. Thus, it is proposed to analyze the stability from the approximation $G_{\text{COFPR}\sim}(s)$. In this sense, any stability analysis technique can be used once the approximation is obtained.

IV. RESULTS

A. SIMULATIONS

1) APPROXIMATION OF THE COFPR CONTROLLER

Following the mentioned steps in Section III-C, from Fig. 6, it is selected to use α equal to 1.5 and β equal to 0.05. This β value reduces the excitation from 5% in the FPR controller case to less than 0.1% in a COFPR controller. The delay at 2000 Hz is moved from 17° to 15°. Consider $[\omega_l, \omega_h] = [20, 10^4]$ Hz and order N equal to 3 and 4. The obtained approximation for

$$G_{\text{COFR}}(s) = \frac{s^{1.5+j0.05}}{(s^2 + (100\pi)^2)} \tag{21}$$

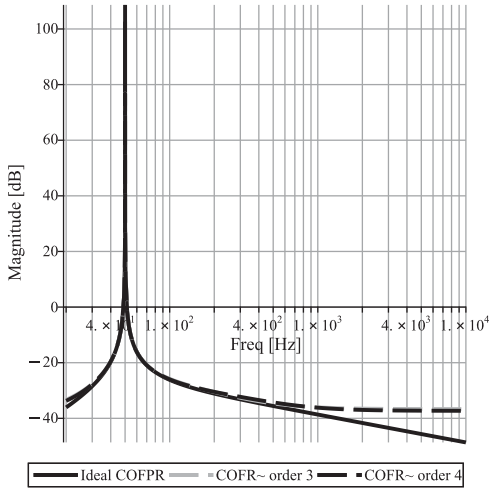

(a)

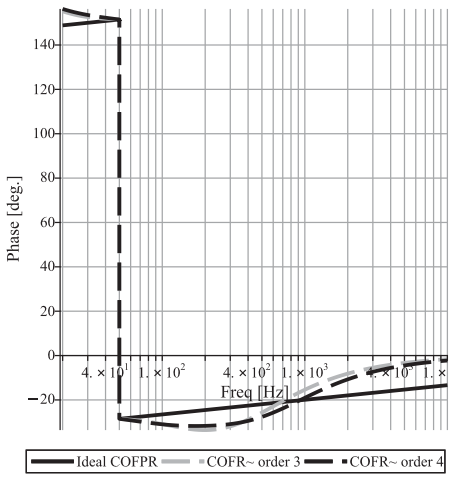

(b)

FIG. 11. Bode diagrams for the COFR controller proposed in (21) for different-order approximation suggested in (22) and (23). (a) Gain. (b) Phase.

in the case of order 4 yields

$$G_{\text{COFR}\sim_3}(s) = \\ = \frac{0.01463(s+2613)(s+223.6)(s-109.1)}{(s+907.7)(s^2+9.87e04)} \tag{22}$$

and for order 5

$$G_{\text{COFR}\sim_4}(s) = \\ = \frac{0.0136(s+3968)(s+914.3)(s+189.4)(s-105)}{(s+1967)(s+536.9)(s^2+9.87e04)}. \tag{23}$$

The approximation strategy is based on minimizing the sum of the squared errors between the desired approximated model and H, (20), from prefixing the number of zeros and poles, which for the presented case will be the same. Fig. 11 depicts

TABLE 4. GM and PM for Different β Values When Used in COFPR Controllers (Tuned According to Section III-A)

Controller	GM	Frequency $_{GM}$	PM	Frequency $_{PM}$
G_{COFR}	∞	Not apply	86.3 deg	36771 Hz
$G_{\text{COFR}_1\sim_4}$	∞	Not apply	89.7 deg	61626 Hz
$G_{\text{COFR}_1\sim_5}$	∞	Not apply	89.3 deg	59127 Hz

the ideal Bode diagram of the controller proposed in (21) and the obtained approximations, defined by (22) and (23). It can be seen that the approximation obtained for orders 3 and 4 are really similar in terms of frequency response. Both approximations offer less than positive 3 dB of error up to about 2 kHz. The maximum lag introduced by (23) is less than 9°. Thus, for the study case, the order 4 approximation defined in (23) is assumed valid and will be applied hereinafter.

2) SIMULATIONS WHEN SAME CONTROLLERS GAINS ARE CONSIDERED

In this section, a set of simulations is conducted in the continuous time domain. This section focuses on the criteria of maintaining the same controllers' gain values, as proposed in Section III-A.

As an example, in terms of stability, the two approximations proposed in Section IV-A1 and the ideal COFPR controller are compared in Table 4 and in the open-loop bode diagrams depicted in Fig. 12. The ideal and approximated transfer functions offer a similar PM when the gain is equal to 0 dB.

The FR$\sim$ and COFR$\sim_4$ (hereinafter COFR$\sim$) controllers proposed are evolved to their corresponding PR forms, FPR$\sim$ and COFPR$\sim$ using k_p set at 2 and k_i set at 200.

Fig. 13 collects the continuous-time Bode diagrams for the closed-loop systems of the controllers and plant presented in Section II-D. As the FPR controller has the same issue of being nonimplementable, the approximation using the same procedure and order 4 defined for the COFPR approximation yields

$$G_{\text{FR}\sim}(s) = \frac{145.64s(s+95.35)(s+1974)}{(s^2+98700)(s+9153)(s+496.5)}. \tag{24}$$

In Fig. 13, it can be seen from the phase diagram that the approximation of the controllers suits better up to about 2000 Hz. Within this range, the FPR$\sim$ controller presents a maximum amplification of 10% with $-17°$, the COFPR$\sim$ controller shows a 0.4% of amplification with $-12°$, and the PRHC offers 3.2% amplification with $-27°$. FPR$\sim$ and COFPR$\sim$ controllers are superior, acting as full-range controllers. In contrast, PRHC is better (practically perfect) just at the controlled toned frequencies. However, it should be noted that the control quality applies to the full frequency range.

Looking deeply at Fig. 13, it is possible to see that the FPR$\sim$ controller presents a resonance peak at about 2.5 kHz of 11%. In contrast, in the case of the COFPR$\sim$ controller, the resonance is practically extinguished, 0.36% at 750 Hz. The high amplification region present for FPR controllers is one of their main drawbacks when using such controllers in real systems where these frequencies can be present. Note that

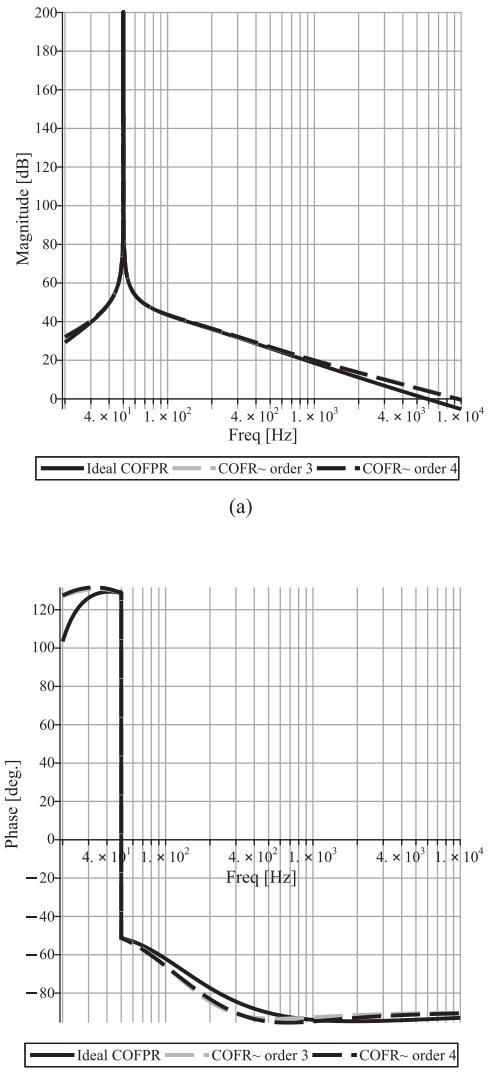

FIG. 12. Open-loop Bode diagrams using controllers proposed in Fig. 11 (assuming $\alpha = 1.5$, $\beta = 0.05$, $k_1 = 2$, and $k_2 = 200$). (a) Gain. (b) Phase.

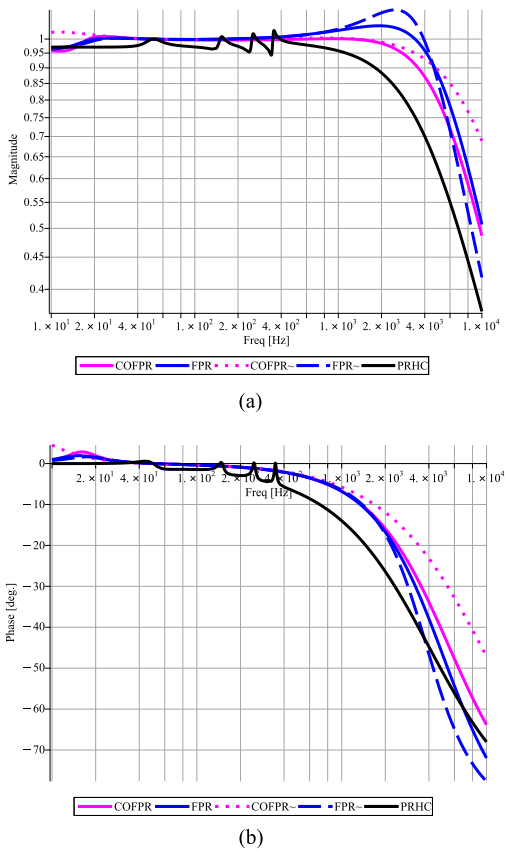

FIG. 13. Closed-loop Bode diagrams for the COFPR, the FPR, and their approximations (assuming $\alpha = 1.5$, $\beta = 0.05$, $k_1 = 2$, and $k_2 = 200$) and the PRHC controller. (a) Gain. (b) Phase.

the proposed COFPR controller can practically extinguish the excitation region.

All the FPR∼, COFPR∼, and PRHC controllers are simulated by MATLAB and compared. Figs. 14–16 gather this comparison considering that different harmonic components of 1 A are referenced at time 0.2 s. Figs. 14 and 15 are related to low-frequency components, the fundamental component (50 Hz), and the fifth harmonic. These cases have no clear advantage for the FPR∼ or COFPR∼ controllers regarding gain or phase tracking, not even in settling time significantly. However, the higher the harmonic component to control, the better the tracking capability and settling time of the FPR∼ or COFPR∼ controllers. Fig. 16 (1000 Hz) shows that the COFPR and FPR controllers exhibit a better tracking performance than the PRHC controller. As a reminder, the PRHC controller is tuned at 50, 150, 250, and 350 Hz. Thus, an important steady-state error appears mainly due to phase error. Fig. 17 represents the effect of a unitary disturbance at 2.5 kHz (closed-loop resonance of the FPR∼) of 10% concerning the fundamental 50 Hz reference. It can be observed that COFPR∼ reduces the error obtained in the PRHC controller by a factor of 2 and the error obtained in the FPR∼ controller by a factor 1.3.

The attenuation of the amplification region provided by the COFPR controller, compared to FPR controllers, is a highly valuable feature for controlling systems with high-order filters such as *LCL* filters. In these *LCL* filters, specific frequencies may emerge, and the control should avoid exciting them.

3) SIMULATIONS WHEN TUNED BY PM IS CONSIDERED

A similar comparison can be made as the one addressed in the previous section. However, the main difference will arise at 225 and 1500 Hz, the peak gain for the PR controllers depicted in Fig. 10, where the tuning criteria were based on PM values. Thus, the two PR controllers are now tuned according to Section III-B. The controller's gains are listed in Table V. In this case, the FPR controller is out of the analysis because it will not include any difference in the results with respect to Section IV-A2.

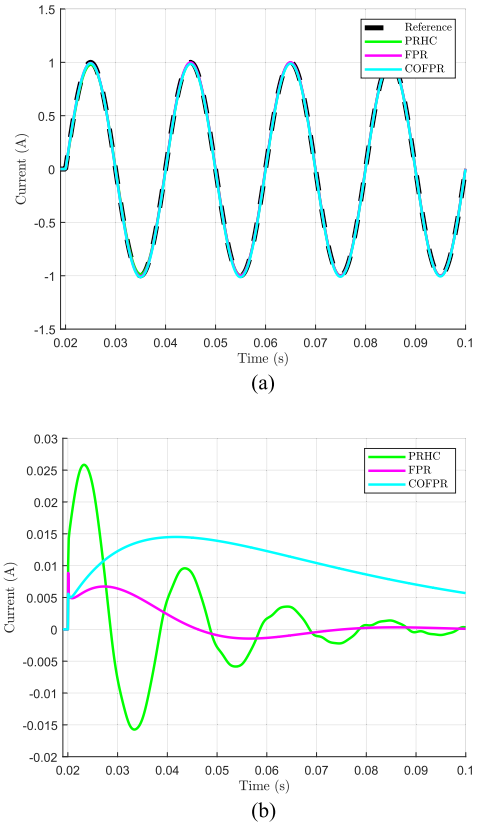

FIG. 14. Step response of PRHC, FPR∼, and the COFPR∼ for 50 Hz reference (tuning procedure according Section III-A). (a) Time response. (b) Error.

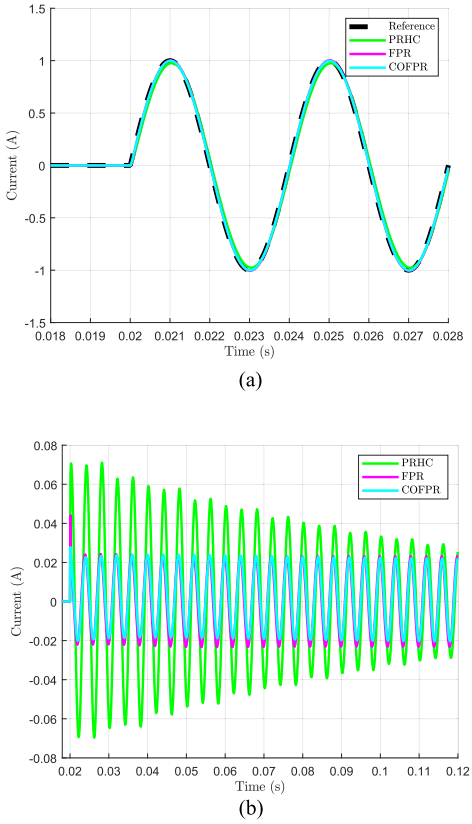

FIG. 15. Step response of PRHC, FPR∼, and the COFPR∼ for 250 Hz reference (tuning procedure according Section III-A). Time response is depicted when $t \in (0.018, 0.028)$ s and error when $t \in (0.018, 0.12)$ s. (a) Time response. (b) Error.

TABLE V Controller's Gains Tuned by PM

Controller	k_p	k_i
COFPR	2.0	200.0
PR_{PM1KHz}	0.49	649.2
PR_{PM8KHz}	4.0	20620

Figs. 18 and 19 illustrate the tracking capability and error for the 1-A peak current reference set at 225 and 1500 Hz, respectively. In Fig. 18, it can be seen that the PR tuned with the same PM as the COFPR∼ controller at 1 kHz provides excessive gain and error margin. As a correction action, the PR tuned by PM at 8 kHz improves the provided bandwidth but at the cost of amplifying a frequency range from 200 to 3.5 kHz. Fig. 19 illustrates this case at the worst scenario for the system under consideration. Note that the error difference between the COFPR∼ controller and the PR controller tuned at 8 kHz is quite similar, but the COFPR∼ controller is more related to phase rather than gain. This fact exemplifies that the excitation region is under control when COFPR∼ is used. Furthermore, from Table V, it can be deduced that the COFPR∼ controller needs a proportional gain half of the PR controller tuned at 8 kHz, making the FPR∼ controller less sensitive to an instantaneous reference change.

As in the previous section, a unitary voltage disturbance at the peak resonance of the worst controller is conducted, now being at 1.5 kHz, as shown in Fig. 10. Fig. 20 depicts the results showing that the PR controller tuned at 8 kHz, and COFPR∼ offers better disturbance rejection, being quite similar at the studied frequency.

B. EXPERIMENTAL RESULTS

1) SETUP

This section presents the implementation of the COFPR∼ controller and compares its performance with that of the FPR∼ and PRHC controllers on a real platform. The COFPR∼ controller and all other controllers used for comparison have been implemented in a Texas Instruments DSP, specifically TMS320F28379DPTPT (32 bits floating DSP), and it has been tested with a 3.6-kVA single-phase bridgeless Totem-Pole GaN-based inverter. The sampling and switching frequency of the inverter are set to 120 kHz. All experimental plots (see Figs. 26 and 27) have been obtained by acquiring real data at 125 kHz from a DL9040 Yokogawa oscilloscope for a 10-s time window. The current probe is a Fluke i30s. All plots from the gathered data were depicted using MATLAB. A picture of the converter setup can be seen in Fig. 21.

The experimental parameters of the plant and the discretization method considered are collected in Section II-D. Thus, the output inductance of the inverter is short-circuited. This

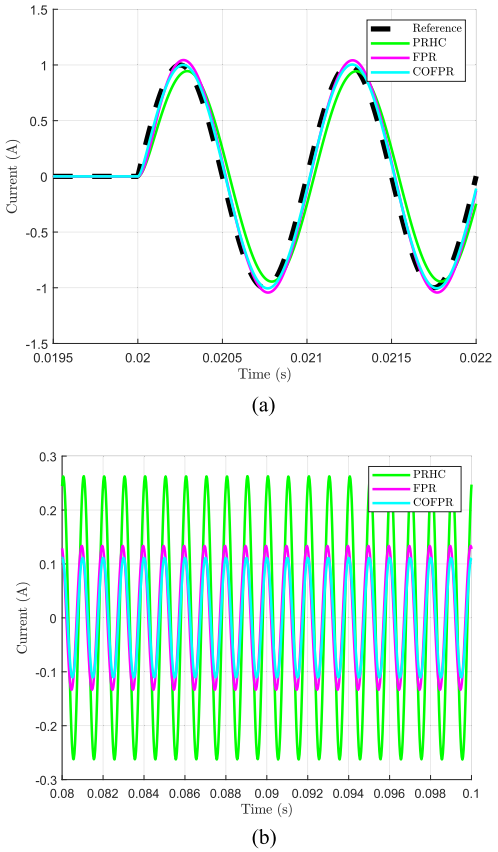

FIG. 16. Step response of PRHC, FPR∼, and the COFPR∼ for 1000 Hz reference (tuning procedure according Section III-A). Time response is depicted when $t \in (0.0195, 0.022)$ s and error when $t \in (0.08, 0.1)$ s. (a) Time response. (b) Error.

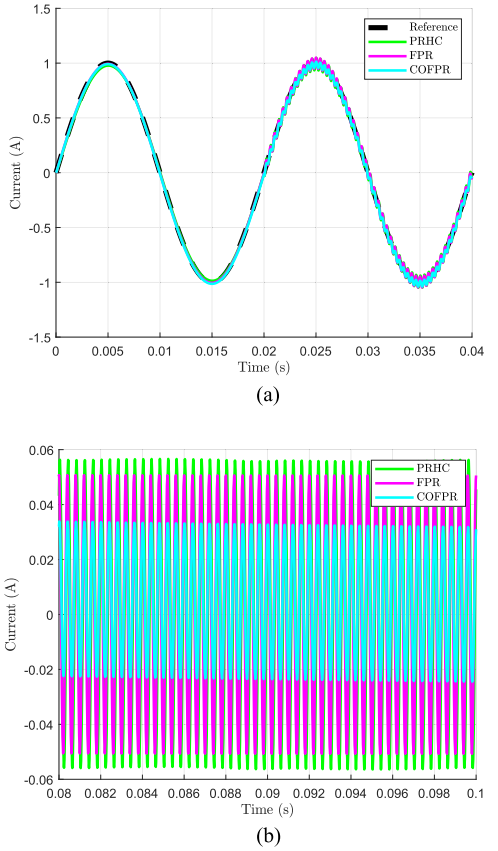

FIG. 17. Step response of PRHC, FPR∼, and the COFPR∼ under a disturbance of 2500 Hz reference (tuning procedure according Section III-A). Time response is depicted when $t \in (0.0, 0.04)$ s and error when $t \in (0.08, 0.1)$ s. (a) Time response. (b) Error.

way, testing the different controllers under low-voltage control actions is possible. The L–R_L impedance is approximately 35 mΩ at 50 Hz or 1 Ω at 2000 Hz. Similar results can be obtained if the inverter is connected to a grid and the controller's output is added to the measured grid voltage. The effect of the voltage disturbance has been analyzed in the Simulations section, as depicted in Figs. 17 and 20.

2) CONSIDERATIONS OF THE REAL SYSTEM

The bilinear transformation

$$s = \frac{2(z-1)}{T_s(z+s1)} \tag{25}$$

discretizes all the controllers, the COFPR∼, FPR∼, PRHC, PR PM 1 kHz, and PR PM 8 kHz.

Fig. 22 compares the Bode diagrams for the COFPR∼ and FPR∼ proposed for the continuous and discrete time. The figure shows that the discretization process does not affect the stability due to gain, and phase curves exhibit a proper match between the time domains. Fig. 23 complements the validation of the discretization process, showing that both the continuous- and discrete-time closed loops suit up to 20 kHz.

3) RESULTS

Two current signals are proposed to be tracked to evaluate the superiority of the COFPR controller.

1) A highly multiharmonic signal based on a controlled frequency number of terms to generate a "Square" set-point signal. The "Square" reference follows the Fourier decomposition shown in Fig. 24. The current signal is based on

$$\begin{aligned} i_L^*(t) = {} & 15(\sin(u) + (1/3)\sin(3u) + (1/5)\sin(5u) + \\ & + (1/7)\sin(7u) + (1/9)\sin(9u) + (1/11)\sin(11u) + \\ & + (1/13)\sin(13u) + (1/15)\sin(15u) + \\ & + (1/25)\sin(25u) + (1/25)\sin(50u)) \end{aligned} \tag{26}$$

with u being an angular frequency of 100π rad/s and i_L^* is the current reference.

2) A highly multiharmonic signal based on a "Batman" with unknown frequencies and a base period of 6.6 ms. The "Batman" reference follows the Fourier decomposition shown in Fig. 25.

Fig. 26 illustrates the "Square" time response tracking ability of the COFPR∼, FPR∼, PRHC, PR PM 1 kHz, and PR

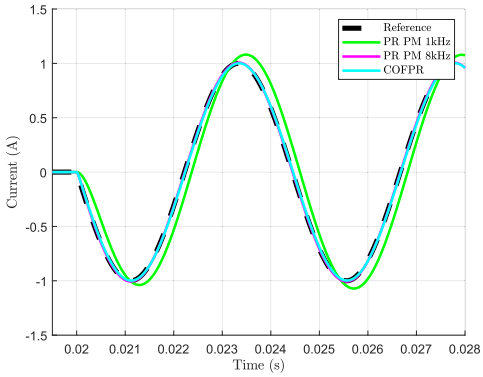

(a)

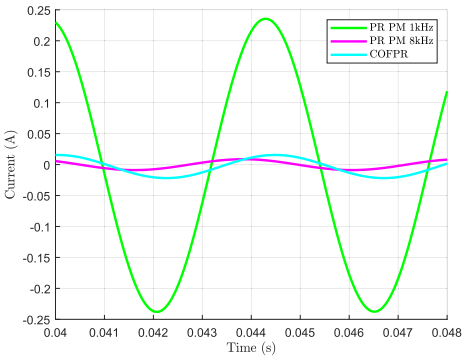

(b)

FIG. 18. Step response of PR PM 1 kHz, PR PM 8 kHz, and FPR∼ for 225 Hz reference (tuning procedure according Section III-B). Time response is depicted when $t \in (0.0195, 0.028)$ s and error when $t \in (0.04, 0.048)$ s. (a) Time response. (b) Error.

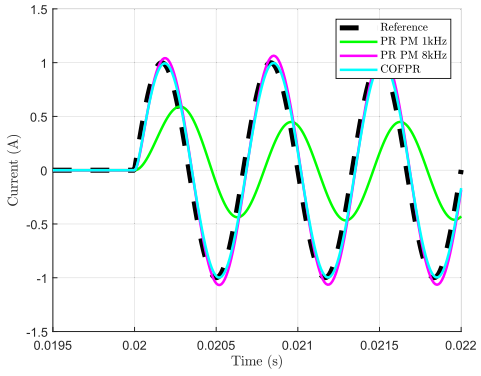

(a)

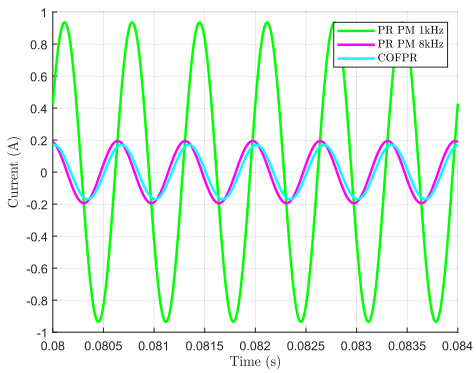

(b)

FIG. 19. Step response of PR PM 1 kHz, PR PM 8 kHz, and FPR∼ for 1500 Hz reference (tuning procedure according Section III-B). Time response is depicted when $t \in (0.0195, 0.022)$ s and error when $t \in (0.08, 0.084)$ s. (a) Time response. (b) Error.

PM 8 kHz controllers developed in Sections III-A and III-B. In this case, and also referring to Fig. 13, it results in a slight and insignificant difference in using one or other controllers for the case of the COFPR∼, FPR∼, and PRHC. However, the PR PM 1-kHz controller exhibits an attenuation behavior, and the PR PM 8 kHz shows an oscillation transient, as illustrated in the zoom box.

However, for applications in which high frequencies are determinant, the difference between controllers' capabilities starts to emerge. Fig. 27 illustrates the "Batman" time response tracking ability of the different controllers under comparison. Clearly, the PRHC and the PR PM 1-kHz controllers exhibit poor time response and natural oscillations and, thus, cannot properly control a wide range of frequencies. Although the COFPR∼, FPR∼, and the PR PM 8-kHz controllers appear to perform similarly, they have significant differences. The COFPR∼ controller consistently maintains the requested "Batman" shape more effectively. This is particularly visible at time 3, 3.1–3.5 (the flat part of the head), 3.7 (the start of the right shoulder), and 4.8 s (the start of the right-wing). Furthermore, in the case of the PR PM 8-kHz controller, there appears some oscillations, and there is a more pronounced excitation (ears). In all these instances, the COFPR∼ controller exhibits less error. In Fig. 28, an fast Fourier transform for the frequency range [2000, 3000] Hz can be seen for the COFPR∼ and FPR∼ controllers (all PR controller options are excluded for clarity due to the presence of oscillations in the time response). In terms of gain, it can be seen that the COFPR∼ can track better for the high-frequency range without producing an excitation, as does the COFPR∼ controller.

TABLE VI Controller Type Comparison in Execution Time and Program Memory Data

Controller type	Execution time (μs)	Program memory (bytes)
COFPR∼	0.675	120
FPR∼	0.675	120
PR (0 HC)	0.451	55
PRHC (3 HC)	0.877	143
$PRHC_2$ (6 HC)	1.493	235

4) COMPUTATION BURDEN

This section compares the controllers used across the experimental implementation regarding computation burdens. Two criteria are used: execution time and program memory. Table VI collects the obtained results when the controllers are implemented in a TMS320F28379DPTP DSP. The PRHC

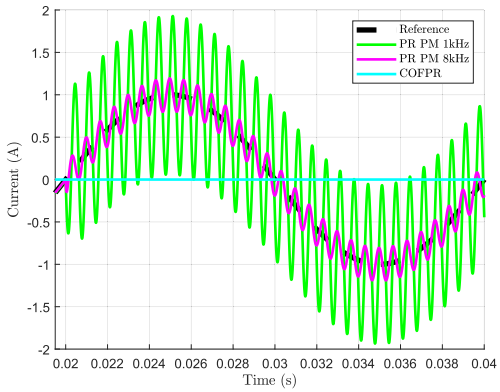

(a)

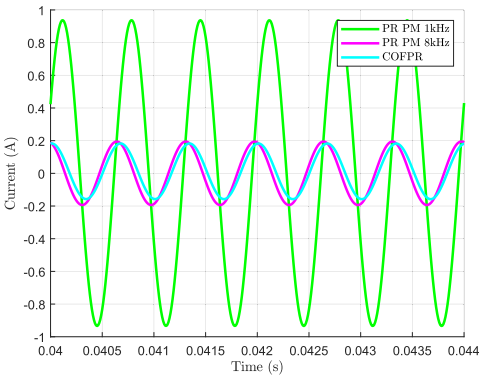

(b)

FIG. 20. Step response of PR PM 1 kHz, PR PM 8 kHz, and FPR∼ under a disturbance of 1500 Hz reference (tuning procedure according Section III-B). Time response is depicted when $t \in (0.0195, 0.04)$ s and error when $t \in (0.04, 0.044)$ s. (a) Time response. (b) Error.

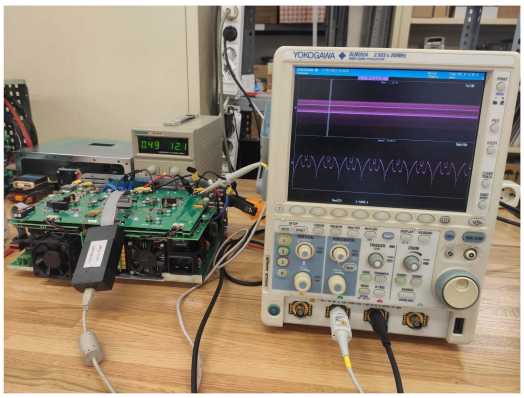

FIG. 21. Picture of the GaN inverter used for the experimental results showing one of the setpoints to track ("Batman" setpoint).

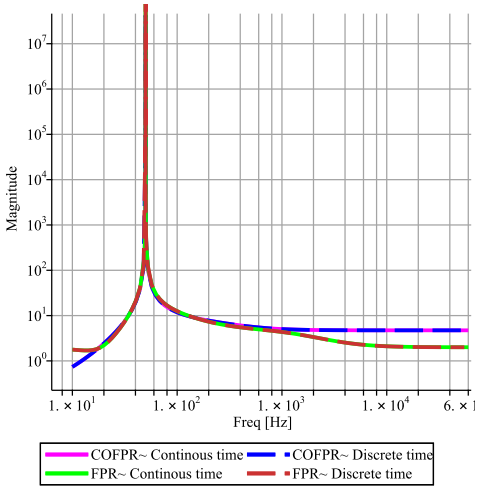

(a)

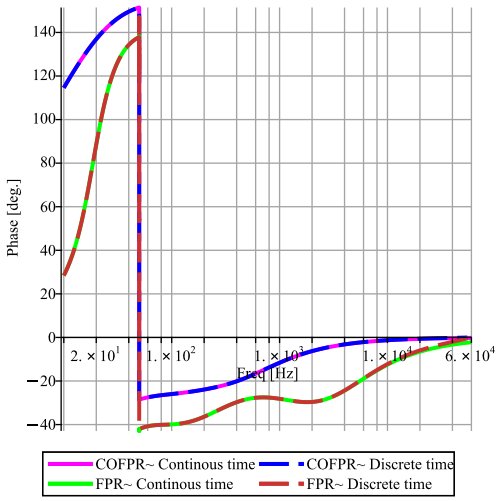

(b)

FIG. 22. Bode diagram of the COFPR and FPR approximation for the continuous and discrete times. (a) Gain. (b) Phase.

controller used in this article considers three HCs to be comparable in terms of order with the FPR and COFR controller alternatives. Also, a new PRHC has been implemented, considering up to six HCs for computational burden reasons. Regarding the criteria selected, the COFPR∼ and FPR∼ fill the same place (same memory and execution time). Both fractional options are superior, using less memory and computational time than other PRHC controller alternatives.

On the one hand, it should be remarked that in terms of execution time, as the sampling frequency is set to 120 kHz, the COFPR controller supposes about 8% (0.675 μs/8.3 μs) of the available computational time for the control task. Conversely, the PRHC (three-HC) controller is about 11% (0.877 μs/8.3 μs), and the PRHC (six-HC) controller is about 18% (0.1493 μs/8.3 μs). Note that for three-phase four-wire applications, these percentages are multiplied by a factor of 3, one for each controller per phase. This last statement is especially sensitive.

In the same direction, assuming each HC in a PRHC controller adds a proportional time (comparing PRHC (three HCs) and PRHC (six HCs) in Table VI), it is possible to conclude that when execution time is limited, the use of PRHC

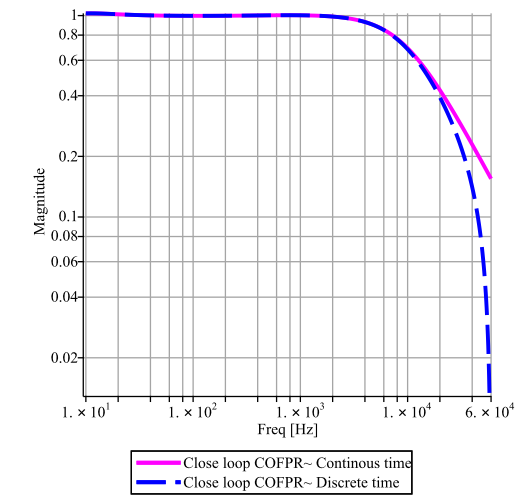

FIG. 23. Closed-loop Bode diagram of the COFPR approximation for the continuous and discrete time. (a) Gain. (b) Phase.

controllers is restricted. For example, as the controller operates at 120 kHz for the case study, a PRHC controller with harmonic compensation up to the 27th harmonic (1350 Hz) is the maximum suitable for three-phase applications, setting the control interruption resting time to zero and, consequently, not leaving any extra time for other tasks.

Therefore, any advanced low-order controller option, such as the proposed COFPR controller, can minimize execution time by allocating the saved time for other critical tasks, such as generating real-time alarms.

V. DISCUSSION

This section aims to summarize and highlight the key points discussed in this article from a qualitative perspective. Specifically, factors such as ease of tuning, controllable bandwidth,

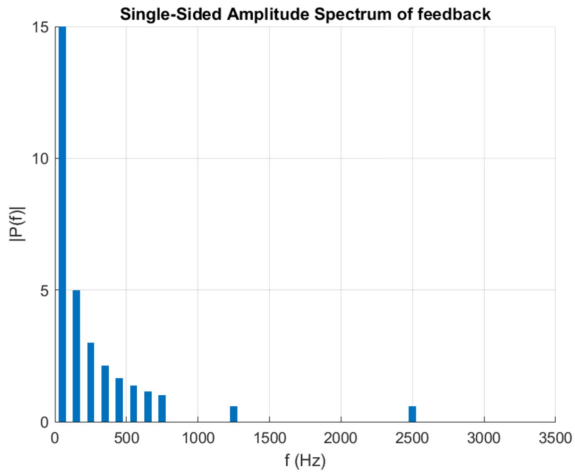

FIG. 24. Fast Fourier transform of the "Square" signal requested.

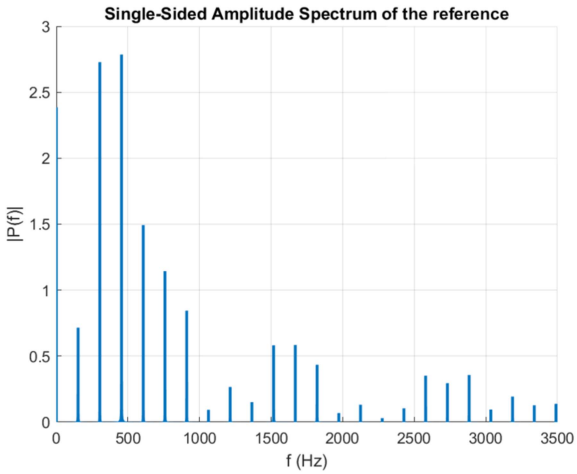

FIG. 25. Fast Fourier transform of the "Batman" signal requested.

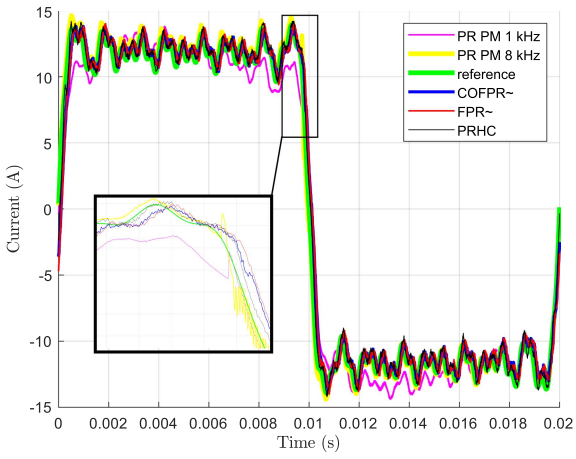

FIG. 26. Comparison of the tracking capability of COFPR~, FPR~, PRHC, PR PM 1-kHz, and PR PM 8-kHz controllers for the "Square" signal reference. Black square represents a zoom box.

TABLE VII Controller's Qualitative Comparison

Specification	PR	PRHC	FPR~	COFPR~
Ease of tuning	High	Medium-High	Medium	Medium-low
Controllable bandwidth	Low-High *	High	Medium-high	Medium-high
Control harmonics	Low-High*	Medium	Medium	Medium
Stability	Low-High*	High	Medium	Medium
Disturbance rejection	Medium	Low	Low	Medium
Program memory	Low	High	Low	Low
Execution time	Low	High	Low	Low

* According to tuning criteria

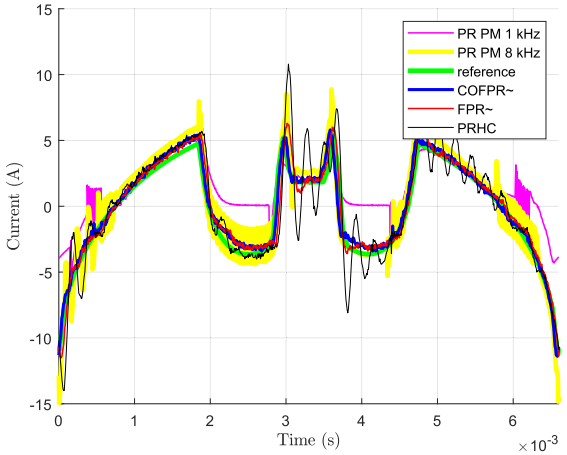

FIG. 27. Comparison of the tracking capability of COFPR~, FPR~, PRHC, PR PM 1-kHz, and PR PM 8-kHz controllers for the "Batman" signal reference.

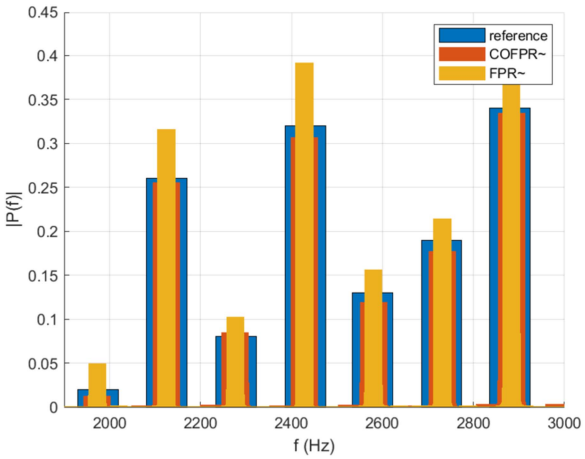

FIG. 28. Fast Fourier transform comparison of the tracking capability of COFPR~ and FPR~ for the "Batman" signal reference for the frequency range [2000, 3000] Hz.

control of specific harmonic tones, stability, disturbance rejection, program memory, and execution time are compared in Table VII.

On the one hand, the PR and PRHC controllers have been widely used for harmonic control. Tuning the PR or PRHC controller primarily involves determining the appropriate proportional and resonant gains. These controller gains can be tuned according to different alternatives, such as the same values based on the same dynamics at a fundamental frequency or by PM criteria, i.e., robustness. For the case of the same controller gains, the FPR and COFPR controllers are better options in terms of tracking capability. In the case of using PM as tuning criteria, the difference is closer in tracking capabilities. Note that the PR, PRHC, or FPR controller traditionally shows a not desired excitation region that the complex term of a COFPR controller can correct. The cost of using the COFPR is mainly due to the approximation requiring a certain order to be a proper solution. However, it has been determined that order 3 or 4 is enough for the approximation, being close to an ideal PR controller of order 2 regarding computation burdens. The tracking capability of a PRHC controller can also be enhanced by incorporating a greater number of HCs. Increasing the number of HC is constrained by the computational capabilities of the processor used for implementation, but each extra HC requires extra execution time and program memory. As an initial result, the PR tuned by high bandwidth PM, the FPR and COFPR controllers demonstrate superior tracking capabilities with reduced computational demand, which can also enhance disturbance rejection. But, as mentioned, the PR and FPR controllers trend to excite some frequency regions.

On the other hand, including one extra degree of freedom in the FPR controller and two extra degrees of freedom in the COFPR makes tuning the controllers more challenging. In addition, it should be noted that both the FPR and COFPR controllers require approximation techniques for implementation, and stability must be ensured based on the strategy employed. As a second partial outcome, the FPR and COFPR are more complex to manage but provide additional degrees of freedom to tailor the desired frequency response.

VI. CONCLUSION

This article proposes to use COFPR controllers for ac application on VSCs. Specifically, COFPR controllers are applied to regulating multiharmonic current tracking. The obtained results can be applied to any other first-order system plant in which some magnitude needs to be controlled in a wide frequency range.

The main contribution of this article is to define a novel controller based on applying CO fractional-order calculus into FPR controllers. FPR controllers enhance the frequency tracking behavior of ac references with a low-order transfer function compared with the conventional multiharmonic PRHC controllers. However, PR, PRHC, and FPR controllers exhibit an excitation region that affects the quality of the output current. The COFPR improves PRHC controllers in a

similar way that FPR controllers do. However, the increase in performance is achieved thanks to using the complex term to reduce the excitation region promoted by the noninteger exponent of FPR controllers. This solution is at the cost of moving order 2 of ideal PR controllers, tuned by high-bandwidth PM, to order 3 or 4. In this sense, the COFPR controller emerges as a good tradeoff solution to be implemented in systems where the computational time is critical, memory dependence is important, and tracking a reference with multiple high-order harmonics is a key point reducing any possible excitation region to practically null values. For instance, when the output plant of the system considers not only first-order systems but also high-order coupling filters, such as *LCL* filters. In the *LCL* filter, there appear resonance regions that are required not to be excited.

Regarding implementing the COFPR controller, frequency response data were gathered to develop an implementable model to minimize the error between the approximation and the frequency response.

A set of simulations and experimental tests through an experimental GaN inverter shows that the COFPR controller can improve the performance of FPR and PRHC controllers. This result applies mainly in the high-frequency range avoiding excitation regions with a low-order controller solution, a valid option for applications with a restricted execution time.

REFERENCES

[1] L. R. Limongi, R. Bojoi, G. Griva, and A. Tenconi, "Digital current-control schemes," *IEEE Ind. Electron. Mag.*, vol. 3, no. 1, pp. 20–31, Mar. 2009.

[2] A. R. Monter, E. J. Bueno, A. García-Cerrada, F. J. Rodríguez, and F. M. Sánchez, "Detailed analysis of the implementation of frequency-adaptive resonant and repetitive current controllers for grid-connected converters," *Elect. Power Syst. Res.*, vol. 116, pp. 231–242, 2014.

[3] X. Quan, X. Dou, Z. Wu, M. Hu, and J. Yuan, "Harmonic voltage resonant compensation control of a three-phase inverter for battery energy storage systems applied in isolated microgrid," *Elect. Power Syst. Res.*, vol. 131, pp. 205–217, 2016.

[4] A. Timbus, M. Liserre, R. Teodorescu, P. Rodriguez, and F. Blaabjerg, "Evaluation of current controllers for distributed power generation systems," *IEEE Trans. Power Electron.*, vol. 24, no. 3, pp. 654–664, Mar. 2009.

[5] D. Zammit, C. Spiteri Staines, and M. Apap, "Comparison between PI and PR current controllers in grid connected PV inverters," *Int. J. Elect., Electron. Sci. Eng.*, vol. 8, no. 2, pp. 221–226, 2014.

[6] P. Rani, Shikhar, S. Murugesan, and A. K. Singh, "Modeling and implementation of grid following and grid forming inverters," in *Proc. IEEE 9th Uttar Pradesh Sect. Int. Conf. Elect., Electron. Comput. Eng.*, 2022, pp. 1–6.

[7] E. Rokrok, T. Qoria, A. Bruyere, B. Francois, and X. Guillaud, "Effect of using PLL-based grid-forming control on active power dynamics under various SCR," in *Proc. IEEE 45th Annu. Conf. Ind. Electron. Soc.*, 2019, vol. 1, pp. 4799–4804.

[8] N. Goñi, J. Marcos, M. García, A. García, A. Urtasun, and L. Marroyo, "High-fidelity averaged model of grid-following inverter for stability analysis considering the PLL influence," in *Proc. IEEE 32nd Int. Symp. Ind. Electron.*, 2023, pp. 1–4.

[9] A. G. Yepes, F. D. Freijedo, J. Doval-Gandoy, O. López, J. Malvar, and P. Fernández-Comesaña, "Effects of discretization methods on the performance of resonant controllers," *IEEE Trans. Power Electron.*, vol. 25, no. 7, pp. 1692–1712, Jul. 2010.

[10] C. Lascu, L. Asiminoaei, I. Boldea, and F. Blaabjerg, "High performance current controller for selective harmonic compensation in active power filters," *IEEE Trans. Power Electron.*, vol. 22, no. 5, pp. 1826–1835, Sep. 2007.

[11] F. Hans, W. Schumacher, S.-F. Chou, and X. Wang, "Design of multifrequency proportional–resonant current controllers for voltage-source converters," *IEEE Trans. Power Electron.*, vol. 35, no. 12, pp. 13573–13589, Dec. 2020.

[12] K. Bingi, R. R. Kulkarni, and R. Mantri, "Design and analysis of complex fractional-order PID controllers," in *Proc. IEEE Madras Sect. Conf.*, 2021, pp. 1–6.

[13] I. Podlubny, "Fractional-order systems and PI-lambda-D-mu controllers," *IEEE Trans. Autom. Control*, vol. 44, no. 1, pp. 208–214, Jan. 1999.

[14] M. A. Azghandi, S. M. Barakati, and A. Yazdani, "Impedance-based stability analysis and design of a fractional-order active damper for grid-connected current-source inverters," *IEEE Trans. Sustain. Energy*, vol. 12, no. 1, pp. 599–611, Jan. 2021.

[15] P. Warrier and P. Shah, "Fractional order control of power electronic converters in industrial drives and renewable energy systems: A review," *IEEE Access*, vol. 9, pp. 58982–59009, 2021.

[16] U. M. Al-Saggaf, R. Mansouri, M. Bettayeb, I. M. Mehedi, and K. Munawar, "Robustness improvement of the fractional-order LADRC scheme for integer high-order system," *IEEE Trans. Ind. Electron.*, vol. 68, no. 9, pp. 8572–8581, Sep. 2021.

[17] A. Zafari, M. Mehrasa, S. Bacha, K. Al-Haddad, and N. Hosseinzadeh, "A robust fractional-order control technique for stable performance of multilevel converter-based grid-tied DG units," *IEEE Trans. Ind. Electron.*, vol. 69, no. 10, pp. 10192–10201, Oct. 2022.

[18] R. Stanisławski, M. Rydel, and Z. Li, "A new reduced-order implementation of discrete-time fractional-order PID controller," *IEEE Access*, vol. 10, pp. 17417–17429, 2022.

[19] C. A. Monje, B. M. Vinagre, V. Feliu, and Y. Chen, "Tuning and auto-tuning of fractional order controllers for industry applications," *Control Eng. Pract.*, no. 16, pp. 798–812, 2008.

[20] J. Sahu, P. Satapathy, M. K. Debnath, P. K. Mohanty, B. K. Sahu, and J. R. Padhi, "Automatic voltage regulator design based on fractional calculus plus PID controller," in *Proc. Int. Conf. Comput. Intell. Smart Power Syst. Sustain. Energy*, 2020, pp. 1–4.

[21] R. Trivedi and P. K. Padhy, "Design of indirect fractional order IMC controller for fractional order processes," *IEEE Trans. Circuits Syst. II, Exp. Briefs*, vol. 68, no. 3, pp. 968–972, Mar. 2021.

[22] A. Idir, H. Akroum, S. A. Tadjer, and L. Canale, "A comparative study of integer order PID, fractionalized order PID and fractional order PID controllers on a class of stable system," in *Proc. IEEE Int. Conf. Environ. Elect. Eng./IEEE Ind. Commercial Power Syst. Eur.*, 2023, pp. 1–6.

[23] D. Heredero-Peris, E. Sánchez-Sánchez, C. Chillón-Antón, D. Montesinos-Miracle, and S. Gálceran-Arelláno, "A novel fractional proportional-resonant current controller for voltage source converters," in *Proc. IEEE 18th Eur. Conf. Power Electron. Appl.*, Sep. 2016, pp. 1–10.

[24] M. Haro-Larrode, G. Bergna-Diaz, P. Eguia, and M. Santos-Mugica, "On the tuning of fractional order resonant controllers for a voltage source converter in a weak AC grid context," *IEEE Access*, vol. 9, pp. 52741–52758, 2021.

[25] D. Heredero-Peris, C. Chillón-Antón, E. Sánchez-Sánchez, and D. Montesinos-Miracle, "Fractional proportional-resonant current controllers for voltage source converters," *Elect. Power Syst. Res.*, vol. 168, pp. 20–45, Mar. 2019.

[26] P. Shah and S. Agashe, "Review of fractional PID controller," *Mechatronics*, vol. 38, pp. 29–41, 2016.

[27] O. W. Abdulwahhab, "Design of a complex fractional order PID controller for a first order plus time delay system," *ISA Trans.*, vol. 99, pp. 154–158, 2020.

[28] I. Podlubny, "Fractional differential equations: An introduction to fractional derivatives, fractional differential equations, to methods of their solution and some of their applications," New York, NY, USA: Elsevier, 1999.

[29] A. G. Yepes, F. D. Freijedo, O. López, and J. Doval-Gandoy, "High-performance digital resonant controllers implemented with two integrators," *IEEE Trans. Power Electron.*, vol. 26, no. 2, pp. 563–576, Feb. 2011.

[30] B. Xie et al., "Analysis and improved design of phase compensated proportional resonant controllers for grid-connected inverters in weak grid," *IEEE Trans. Energy Convers.*, vol. 35, no. 3, pp. 1453–1464, Sep. 2020.

[31] F. J. Rodríguez, E. Bueno, M. Aredes, L. G. B. Rolim, F. A. S. Neves, and M. C. Cavalcanti, "Discrete-time implementation of second order generalized integrators for grid converters," in *Proc. IEEE 34th Annu. Conf.*, 2008, pp. 176–181.
[32] C. Monje, Y. Chen, B. Vinagre, D. Xue, and V. Feliu, *Fractional Order Systems and Control—Fundamentals and Applications*. New York, NY, USA: Springer, 2010.
[33] K. Bingi, R. Ibrahim, M. Karsiti, and S. Hassan, "Frequency response based curve fitting approximation of fractional–order PID controllers," *Int. J. Appl. Math. Comput. Sci.*, vol. 29, pp. 311–326, Jan. 2019.
[34] A. Calderón, B. Vinagre, and V. Feliu, "Fractional order control strategies for power electronic buck converters," *Signal Process.*, vol. 86, no. 10, pp. 2803–2819, 2006.

DANIEL HEREDERO-PERIS was born in Vilanova i la Geltrú, Spain, in 1985. He received the M.Sc. degree in control engineering and the Ph.D. degree in electrical engineering from the Technical University of Catalonia (UPC), Barcelona, Spain, in 2010 and 2017, respectively.

Since 2010, he has been a Project Engineer with the Centre d'Innovació Tecnològica en Convertidors Estàtics i Accionaments, UPC, where he develops tasks focused on the design of algorithms related to the control of grid-connected and standalone inverters, and vehicle-to-grid projects. His main research interests include control of power electronics, microgrids, and electric vehicles.

MACIÀ CAPÓ-LLITERAS was born in Menorca, Spain, in 1990. He received the M.Sc. degree in industrial engineering from the School of Industrial Engineering of Barcelona, Barcelona, Spain, in 2014, and the Ph.D. degree in electrical engineering from the Universitat Politècnica de Catalunya (UPC), Barcelona, in 2024.

Since 2014, he has been a Project Engineer with the Centre d'Innovació Tecnològica en Convertidors Estàtics i Accionaments, UPC, where he develops tasks focused on designing power electronics converters. This area involves dual-active-bridge converters for dc–dc isolation, vehicle-to-grid projects for electric vehicles (EVs), and controllers for light electric vehicles. His main research interests include the hardware design with new semiconductor technologies and their control in EV and battery integration.

DANIEL MONTESINOS-MIRACLE (Senior Member, IEEE) was born in Barcelona, Spain, in 1975. He received the M.Sc. and Ph.D. degrees in electrical engineering from the Technical University of Catalonia (UPC), Barcelona, Spain, in 2000 and 2008, respectively.

Since 2001, he has been a Research Collaborator with the Centre d'Innovació Tecnològica en Convertidors Estàtics i Accionaments (CITCEA), UPC. In 2005, he became a Lecturer with the Department of Electrical Engineering, UPC. In 2016, he became the Director of CITCEA, UPC. In 2012, he co-founded TeknoCEA, Barcelona, Spain, a company providing services for power electronics research.

JOAQUIM MELENDEZ-FRIGOLA received the B.S. degree in telecommunication engineering from the Universitat Politècnica de Catalunya, Barcelona, Spain, in 1991, and the Ph.D. degree in electronics, computer science and automatic control from the Universitat de Girona, Girona, Spain, in 1998.

Since 1999, he has been a Professor with the Department of Electrical, Electronic and Automation Engineering, Universitat de Girona, where he is the Director of the Ph.D. Program in Technology and the Director of eXiT, a Research Group on Control Engineering and Intelligent Systems.